The *B*-Matrix Must Be Rotated When Correcting for Subject Motion in DTI Data

Alexander Leemans* and Derek K. Jones

To estimate diffusion tensor MRI (DTI) measures, such as fractional anisotropy and fiber orientation, reliably, a large number of diffusion-encoded images is needed, preferably cardiac gated to reduce pulsation artifacts. However, the concomitant longer acquisition times increase the chances of subject motion adversely affecting the estimation of these measures. While correcting for motion artifacts improves the accuracy of DTI, an often overlooked step in realigning the images is to reorient the *B*-matrix so that orientational information is correctly preserved. To the best of our knowledge, most research groups and software packages currently omit this reorientation step. Given the recent explosion of DTI applications including, for example, neurosurgical planning (in which errors can have drastic consequences), it is important to investigate the impact of neglecting to perform the *B*-matrix reorientation. In this work, a systematic study to investigate the effect of neglecting to reorient the *B*-matrix on DTI data during motion correction is presented. The consequences for diffusion fiber tractography are also discussed. Magn Reson Med 61:1336–1349, 2009.
© 2009 Wiley-Liss, Inc.

Key words: diffusion tensor imaging; white matter; fiber tractography; *B*-matrix reorientation; motion correction; gradient directions

Reliable calculation of diffusion measures, such as fractional anisotropy (FA) and fiber orientation, is important for quantitative diffusion tensor MRI (DTI) analyses, and has been studied extensively with respect to image noise (1–5), eddy current induced distortion artifacts, (6–15), and data reproducibility (16–18). Previous research has also shown that the choice of gradient sampling scheme can affect the precision of the FA and mean diffusivity (MD), suggesting that a larger number of gradient directions (i.e., > 20–30) is required to estimate these diffusion measures robustly (19–26). However, longer acquisition times increase the chances of subject motion, potentially nullifying the benefit of optimizing the gradient acquisition scheme.

When correcting for subject motion, an important step in realigning the diffusion weighted (DW) images is to reorient the corresponding ***B***-matrix so that orientational information is correctly preserved (6). This reorientation step is often neglected, however, when estimating the diffusion tensor and its contribution to the accuracy and precision of DTI measures has not yet been investigated systematically.

Given the recent proliferation of clinical DTI applications, it is important to understand the consequences of neglecting to reorient the ***B***-matrix during motion correction, especially for neurosurgical planning, in which tractography is being introduced as a tool for assessing white matter (WM) architectural configurations (27–29). In this work, we systematically investigated the effect of omitting the ***B***-matrix reorientation on the estimation of diffusion measures, such as the FA, MD, and first eigenvector (FE), during motion correction. The adverse consequences for diffusion fiber tractography (both deterministic and probabilistic approaches) are also demonstrated.

METHODS

Definitions and Notations

Consider K DW images S^k ($k = 1, \ldots, K$) along gradient directions $\boldsymbol{g}^k = [g_x^k g_y^k g_z^k]^t$ with a constant b-value (S_0 is the non-DW image). After realigning the images S^k to S_0, i.e., $\hat{S}^k = \boldsymbol{A}^k(S^k)/|J(\boldsymbol{A}^k)|$ with $\boldsymbol{A}^k$ the affine transformation and $|J(\boldsymbol{A}^k)|$ the Jacobian determinant of $\boldsymbol{A}^k$, the diffusion tensor $\boldsymbol{D}$ is estimated from

$$\hat{S}^k = S_0 e^{-\sum_{\alpha=x,y,z}\sum_{\beta=x,y,z}\hat{B}^k_{\alpha\beta}D_{\alpha\beta}} \quad [1]$$

with the ***B***-matrices $\hat{\boldsymbol{B}}^k$ now defined by the reoriented gradient directions $\hat{\boldsymbol{g}}^k$, i.e.

$$\hat{\boldsymbol{B}}^k = b\hat{\boldsymbol{g}}^k \cdot (\hat{\boldsymbol{g}}^k)^t = b\boldsymbol{R}^k \cdot \boldsymbol{g}^k \cdot (\boldsymbol{R}^k \cdot \boldsymbol{g}^k)^t = \boldsymbol{R}^k \cdot \boldsymbol{B}^k \cdot (\boldsymbol{R}^k)^t. \quad [2]$$

In Eq. [2], $\boldsymbol{R}^k$ represents the rotation matrix from $\boldsymbol{A}^k$, which is defined here by the rotation angles ϕ_x (anterior-posterior axis), ϕ_y (left-right axis), and ϕ_z (inferior-posterior axis) (see Appendix A).

We denote the eigenvalue-eigenvector pairs obtained from the diffusion tensor eigenvalue decomposition as $(\boldsymbol{e}_i^r, \lambda_i^r)_{i=1,2,3}$, the fractional anisotropy as FA_r, the mean diffusivity as MD_r, and the transverse diffusivity (TD) as $TD_r = (\lambda_2^r + \lambda_3^r)/2$ when the ***B***-matrix was rotated (see Eq. [2]), and analogously $(\boldsymbol{e}_i^{nr}, \lambda_i^{nr})_{i=1,2,3}$, FA_{nr}, MD_{nr}, and TD_{nr} when the ***B***-matrix rotation was omitted.

The relative statistical bias ε (averaged over N runs) in any of the aforementioned scalar measures M is defined as $\varepsilon_M = \langle (M_r - M_{nr})/(M_r + M_{nr}) \rangle$ and the precision of M is defined by the 95% confidence interval (CI) CI_M. The bias in the FE is described by the angle θ between $\boldsymbol{e}_1^r$ and $\boldsymbol{e}_1^{nr}$, i.e., $\theta = \arccos(|\boldsymbol{e}_1^r \cdot \boldsymbol{e}_1^{nr}|)$. The cone of uncertainty (CoU) of θ, denoted as CoU_θ, is calculated as the angle that defines the 95th percentile from the estimates of θ (22).

Simulations

Monte Carlo simulations were performed to demonstrate the effect of neglecting to reorient the ***B***-matrix on the estimation of diffusion measures when correcting for subject

CUBRIC (Cardiff University Brain Research Imaging Centre), School of Psychology, Cardiff University, Park Place, Cardiff, United Kingdom

*Correspondence to: Alexander Leemans, CUBRIC, School of Psychology, Cardiff University, Park Place, Cardiff - CF10 3AT, United Kingdom. E-mail: LeemansA@cf.ac.uk

Received 27 June 2008; revised 3 October 2008; accepted 19 October 2008.

DOI 10.1002/mrm.21890

Published online 24 March 2009 in Wiley InterScience (www.interscience.wiley.com).

© 2009 Wiley-Liss, Inc.

motion. Without loss of generality, when referring to *subject motion*, a rotational component is assumed to exist. In addition, because translation parameters do not affect the ***B***-matrix rotation they are not incorporated in this framework.

Diffusion tensors were simulated in the same way as described in Ref. 5. In summary, axially symmetric diffusion tensors were predefined by specifying the FA, MD, and the FE. Next, given a particular b-value and non-DW signal S_0, the corresponding DW signals $\hat{S}^k$ for a specific set of *correct* gradient directions $\hat{\boldsymbol{g}}_k$ were calculated from Eq. [1]. To simulate the effect of omitting the ***B***-matrix rotation for DW image $\hat{S}^k$, the gradient $\hat{\boldsymbol{g}}_k$ was substituted in Eq. [1] by the *incorrect* diffusion gradient $\boldsymbol{g}_k$, which reflects the change in head orientation. Subsequently, the difference between the diffusion tensor—as estimated from Eq. [1]—and the *correct* predefined diffusion tensor can now be investigated for any subset of directions $\{k = 1, \ldots, K\}$ being corrupted by head motion. Note that such simulations can be performed analogously for diffusion tensors that were computed from measured diffusion data. Finally, the actual subject motion is modeled by defining the diffusion gradients $\boldsymbol{g}_k$. For example, if $\boldsymbol{g}_k = \hat{\boldsymbol{g}}_k$ for $k = 1, \ldots, K$, there was no subject motion. On the other hand, if $\boldsymbol{g}_3 \neq \hat{\boldsymbol{g}}_3$, there was a change in head orientation when measuring S^3. The amount of this change can be predefined by the angle between $\boldsymbol{g}_3$ and $\hat{\boldsymbol{g}}_3$. Further details of the different conditions that were simulated to investigate the effect on the estimation of the diffusion measures when the ***B***-matrix is not rotated during subject motion correction are described in Appendix B.

Data Acquisition

Cardiac-gated DTI data were acquired from 10 healthy volunteers aged 25–35 years (5 males, 5 females) on a GE 3T HDx system with a single-shot spin-echo EPI sequence with the following parameters: b-value = 1200 s/mm^2 along 60 gradient directions; Six non-DW images; FOV = 23 cm; acquisition matrix = 96 × 96; 2.4 mm slice thickness, ASSET factor = 2; 60 axial slices, with effective TR = 15 R-R intervals; total acquisition time = 25 min. All subjects gave written informed consent to participate in this study under a protocol approved by the Cardiff University Ethics Committee.

Data Processing

The tensor model was fitted to the data using the Levenberg–Marquardt nonlinear regression method (30). An affine (12 degrees of freedom) coregistration technique based on mutual information was used to realign the (non-) DW images to the first non-DW image (31). Note that subject motion and global geometrical distortions were corrected simultaneously. A detailed description of this framework can be found in the work of Rohde et al. (6). The model-fit error E—here calculated for each voxel as the normalized median absolute value of the DW residual with respect to the tensor model—is used to indicate the quality of the diffusion tensor fit (lower values reflect a better fit to the data), representing an indirect measure to assess the quality of the motion/distortion correction procedure (14), i.e.

$$E = \underset{k}{\text{median}} \left\{ \frac{\hat{S}^k - S_0 e^{-\sum_{\alpha=x,y,z} \sum_{\beta=x,y,z} \hat{B}^k_{\alpha\beta} D_{\alpha\beta}}}{\hat{S}^k + S_0 e^{-\sum_{\alpha=x,y,z} \sum_{\beta=x,y,z} \hat{B}^k_{\alpha\beta} D_{\alpha\beta}}} \right\}. \quad [3]$$

Prior to applying the correction procedure, this error measure is denoted as $\hat{E}$. Note that E is an independent measure because mutual information was used as the coregistration cost function.

Finally, both a deterministic and probabilistic (based on the wild bootstrap) fiber tractography approach were used to show the fiber pathway differences between rotating and not rotating the ***B***-matrix (32,33). In summary, the following criteria were used for the deterministic approach: step size of 1 mm, angle threshold of 30°, FA threshold of 0.15, fiber tracts with a length smaller than 40 mm where omitted, full brain seeding, and robust multiple ROI selection procedure for reconstructing the tracts of interest. For the probabilistic tractography method, one seed point was defined from which 1000 fiber tract pathways were launched (33). DTI processing and visualization of the fiber tractography results was performed with the toolbox ExploreDTI (http://www.ExploreDTI.com).

RESULTS

Simulations

Amount of Gradient Reorientation

Figure 1a shows the effect of increasing the rotation of a single gradient around the z-axis on the estimation of the FA, MD, the eigenvalues, and the FE. Notice that the nonmonotonic behavior of the bias is different for each of these diffusion measures. In Fig. 1b, the bias is calculated for an entire axial slice. It is clear that this bias is nonuniform and can have local extrema within the small range of $\phi_z = [0^\circ \rightarrow 3^\circ]$.

The typical pattern of subject motion that was observed in our in vivo MR data can be described as a slowly varying change in head orientation, as shown by the rotation angles in the top two rows of Fig. 2a, which were derived from the motion correction procedure. In the bottom two rows of Fig. 2a, the subject motion drift is shown when simulated as a random walk. Although only 10 subjects were used in this study, it is already clear that the pitch tends to be more pronounced than the roll and yaw (bottom image in Fig. 2a).

Analogously with Fig. 1a, the adverse effect of not reorienting the ***B***-matrix for a subject motion drift is shown in Fig. 2b. An important observation is that for specific drift axes and diffusion tensor properties, the bias in the direction of FE can be larger than the maximum rotation angle in the observed drift angles, i.e., $\theta > \delta$.

Rotation Axis of Subject Motion

Figure 3a shows the effect of subject motion along different rotation axes on the estimated diffusion measures. It is clear that the bias due to a yaw (ϕ_z), pitch (ϕ_y), and roll (ϕ_x) is smallest for inferior-superior, left-right, and anterior–posterior oriented fiber structures, respectively, as indicated by the arrows. This difference in bias for

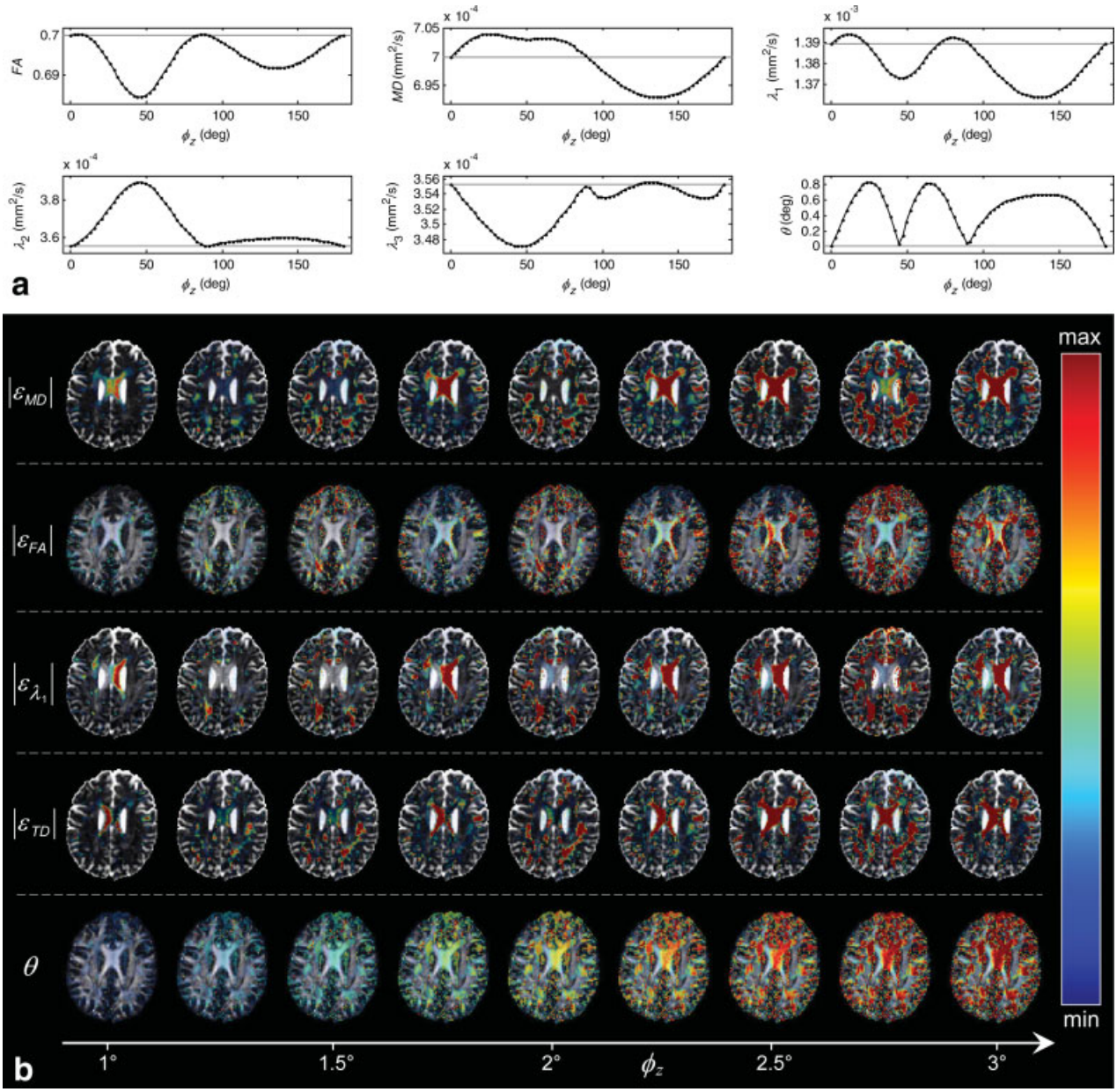

FIG. 1. The effect of not reorienting the ***B***-matrix on the estimation of diffusion measures when rotating a single gradient direction with ϕ_z for (**a**) a single simulated diffusion tensor and (**b**) an axial slice, which was simulated from a measured DTI data set. Note that the color map, which indicates the amount of bias, was scaled differently between—but identically within—each diffusion measure (a linear transparency was applied with the same scale range). [Color figure can be viewed in the online issue, which is available at www.interscience.wiley.com.]

different rotation axes is shown in detail for a single diffusion tensor with $\boldsymbol{e}_1 = [1\,0.5\,0]/\sqrt{1.25}$ in Fig. 3b. Notice that the amount of bias for each rotation axis is dependent on the size of the $\boldsymbol{e}_1$ component along that axis.

A more general overview of the orientational dependency is shown in Fig. 3c-1 and c-2, where the rotation axes $\boldsymbol{a}$ are defined as a uniformly distributed set of points, $\boldsymbol{v}$, on the unit sphere. For a fixed drift pattern $\delta_{\{\boldsymbol{a}\}} = 1°$ with $\boldsymbol{e}_1 = [1\,0\,0]$, the bias in FE orientation, i.e., θ, is larger for rotation axes that form a larger angle with $\boldsymbol{e}_1$. On the other hand, for $\boldsymbol{e}_1 = [1\,1\,1]$, the bias θ shows a more complex pattern, in which its minimum is not found along the rotation axis that is parallel with $\boldsymbol{e}_1$.

In Fig. 3c-3 and c-4, the bias θ is shown for the same fixed drift rotations $\delta_{\boldsymbol{a}=[100]} = 1°$ and $\delta_{\boldsymbol{a}=[111]} = 1°$, respectively, where the first eigenvectors are now defined by the set of points $\{\boldsymbol{v}\}$ on the unit sphere. Again, a non-trivial complex pattern can be observed, which clearly demonstrates that the estimated bias is not rotationally invariant.

Anisotropy and Mean Diffusivity Values

As can be seen from the top row in Fig. 4a, the amount of bias introduced when neglecting the ***B***-matrix reorientation depends on the FA and MD of the diffusion tensor. In addition, the precision of the estimated diffusion measures

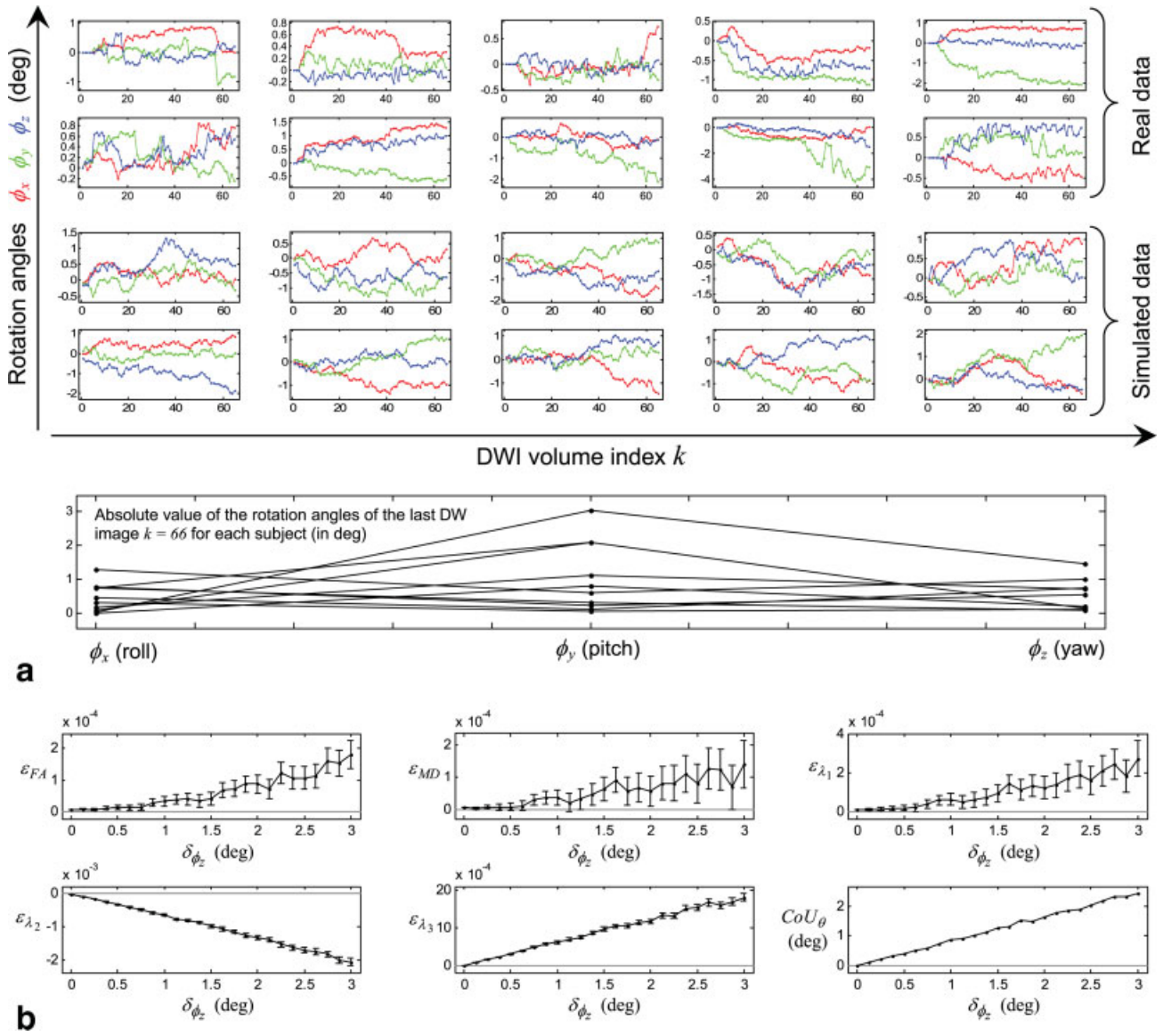

FIG. 2. (**a**) Observed (top two rows) and simulated (bottom two rows) rotation angles reflecting the change in head orientation (subject motion drift) during acquisition of the DW images. The absolute value of the rotation angles ϕ_x, ϕ_y, and ϕ_z obtained from aligning S^{66} to S_0 are also shown for each subject. (**b**) The estimated bias as a function of the amount of drift δ_{ϕ_z} (1000 runs) for the FA, FE, CoU, and the eigenvalues (the error bars represent the 95% CI for 1000 runs). [Color figure can be viewed in the online issue, which is available at www.interscience.wiley.com.]

is affected (see bottom row of Fig. 4a). Note, however, that these patterns of bias and precision as a function of FA and MD will depend on the magnitude and orientation of the motion drift $\delta_{\boldsymbol{a}}$.

Diffusion Gradient Sampling Schemes

For the subject motion with a fixed amount of drift per unit time, the bias in the diffusion measures is generally higher for the sampling schemes with more directions, which is clearly demonstrated for CoU_θ (see Fig. 4b top). On the other hand, for the random subject motion using a fixed amount of rotation for each of the gradient directions, as used in Ref. 34, the effect of the number of gradient directions on the bias is the opposite: a higher bias for fewer directions (see Fig. 4b bottom).

In Vivo DTI Data

In the following sections, the effect of neglecting the ***B***-matrix rotation during motion correction on the estimation of diffusion properties and its consequences for tractography will be presented for an exemplary DTI data set (male aged 29 year).

Correcting Subject Motion

The rotation angles obtained from the motion correction procedure are shown in the bottom left of Fig. 5a. Notice that the predominant drift can be described by the pitch angle (ϕ_y). Also, a qualitative example of the coregistration performance is shown for a sagittal slice of the last DW image, S^{66}, demonstrating the improved alignment

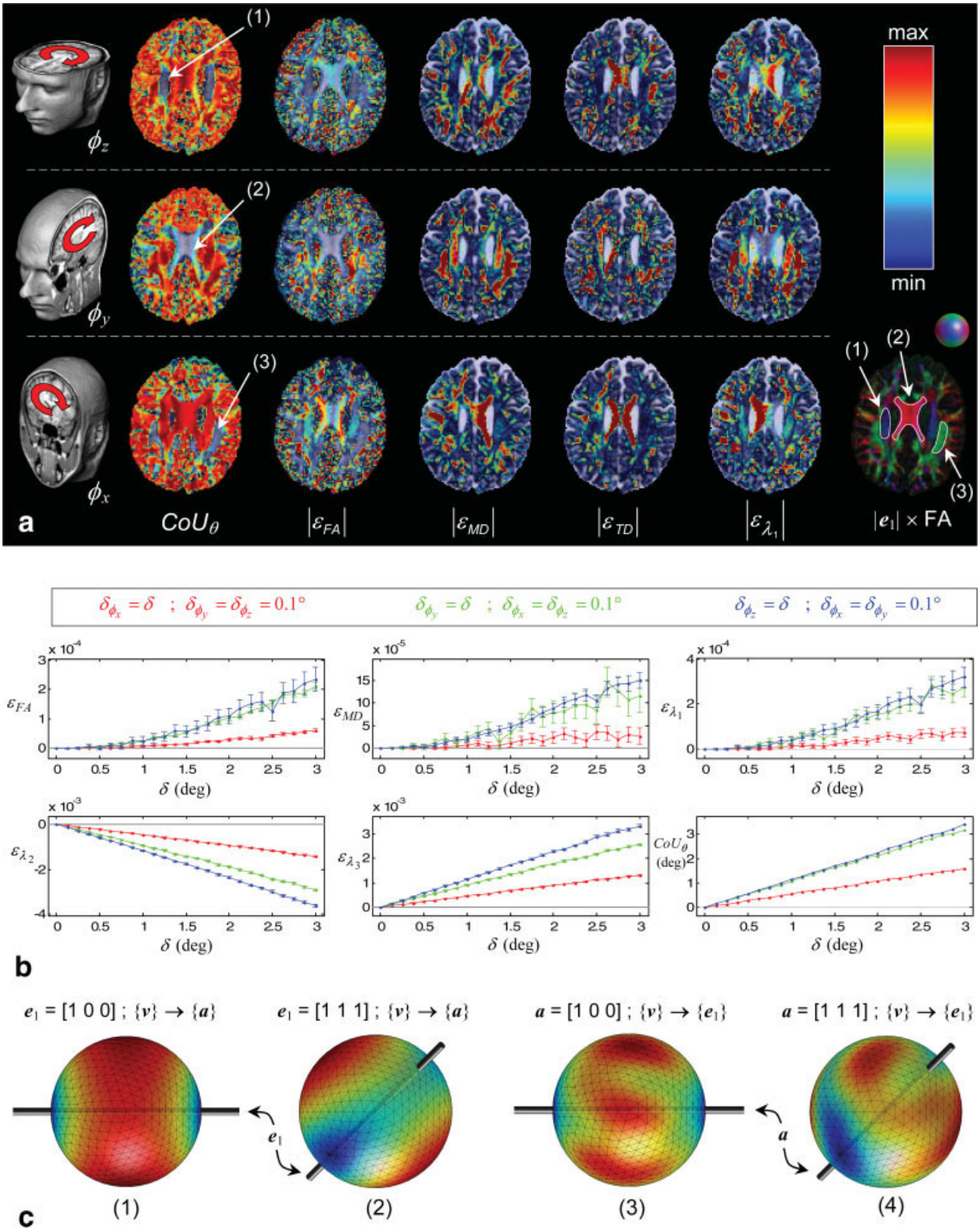

FIG. 3. (**a**) The bias in diffusion measures induced by not reorienting the ***B***-matrix when there was motion in the axial (top row), sagittal (middle row), and coronal (bottom row) image plane (transparency and color scale are defined analogously to Fig. 1b). The arrows in the second column indicate the cortico-spinal tracts (top), the corpus callosum (middle), and superior longitudinal fasciculus, as also shown by the color-encoded FA map (right bottom). (**b**) The bias for a single diffusion tensor with $\boldsymbol{e}_1 = [1\ 0.5\ 0]/\sqrt{1.25}$ as a function of the amount of motion drift δ along the three principal axes. In (**c**), the amount of bias in $\boldsymbol{e}_1$, i.e., θ, is plotted on the unit sphere for a single diffusion tensor (same color bar as in (a), with equal scale for each image). In (1) and (2), the gray lines represent the orientation of $\boldsymbol{e}_1$, and each point ***v*** on the sphere reflects the orientation of the rotation axis ***a*** that defines the motion drift. In (3) and (4), the gray lines indicate the axis ***a***, and the set {***v***} describes the first eigenvectors $\boldsymbol{e}_1$. [Color figure can be viewed in the online issue, which is available at www.interscience.wiley.com.]

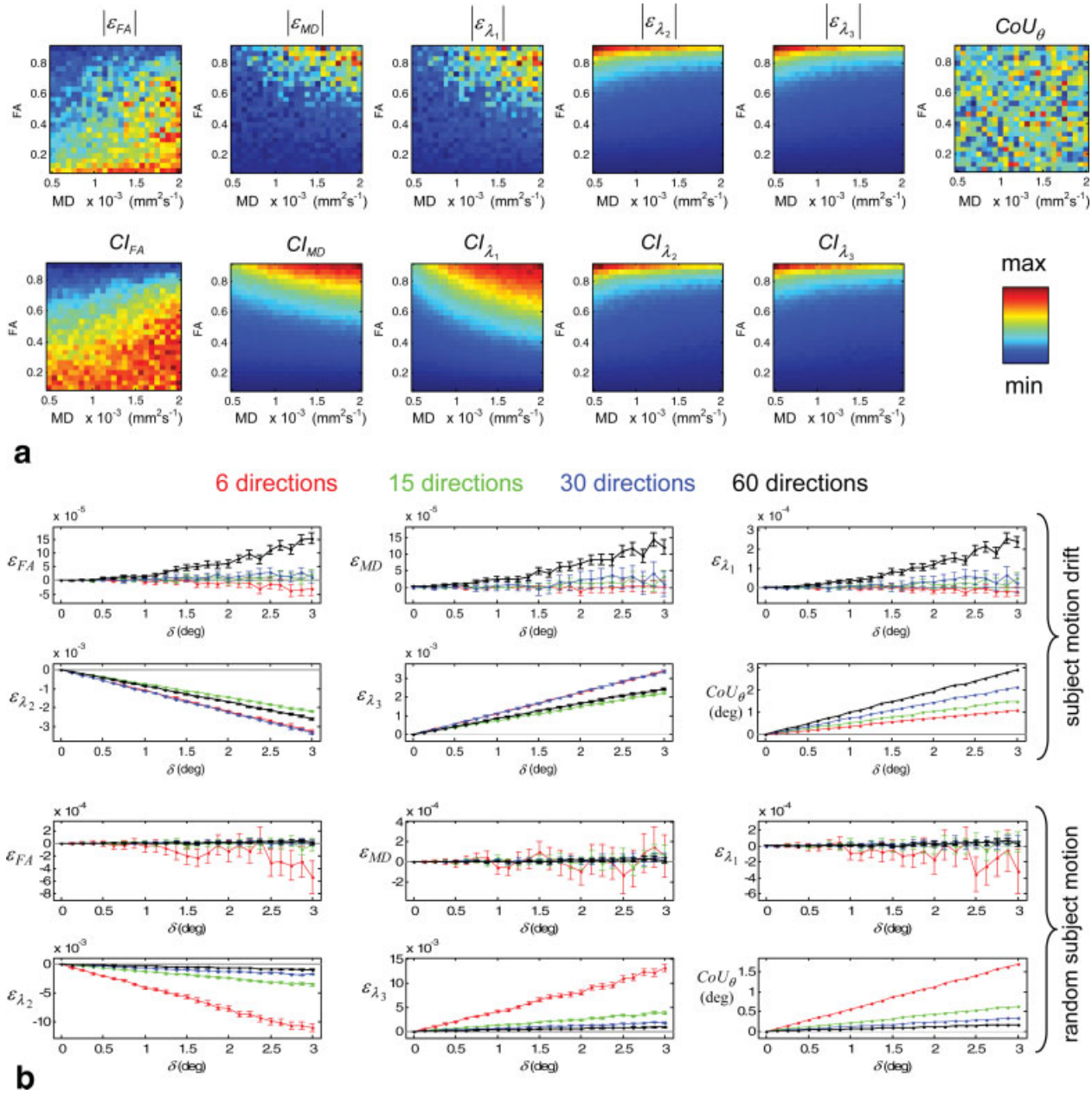

FIG. 4. The bias in diffusion measures induced by not reorienting the ***B***-matrix during motion correction as a function of the FA and MD of the simulated diffusion tensor (**a**), the number of gradient directions for both a subject motion drift and a random subject motion (**b**). Note that the color maps in (a), which indicate the amount of bias or precision, were scaled differently for each diffusion measure. [Color figure can be viewed in the online issue, which is available at www.interscience.wiley.com.]

of $\hat{S}^{66}$ with the non-DW image S_0 (see top row and right column of Fig. 5a). This improvement is highlighted (see encircled regions), demonstrating the higher correspondence of the cortex-CSF interface for $\hat{S}^{66}$. More quantitatively, in Fig. 5a (bottom middle), it is shown that the normalized model-fit error is lower after applying the correction procedure.

Bias in Diffusion Measures

Figure 5b demonstrates the non-uniformity of the bias in the diffusion measures for 6 axial slices. The (two-sided) 1% trimmed bias range for these measures are: $\theta \rightarrow [0.2°, 2°]$; $\varepsilon_{FA} \rightarrow [-0.43, 0.40] \times 10^{-2}$; $\varepsilon_{MD} \rightarrow [-5.9, 4.3] \times 10^{-4}$; $\varepsilon_{\lambda_1} \rightarrow [-9.3, 7.7] \times 10^{-4}$; $\varepsilon_{\lambda_2} \rightarrow [-0.94, 1.2] \times 10^{-3}$; $\varepsilon_{\lambda_3} \rightarrow [-1.7, 2.3] \times 10^{-3}$. To further elucidate the orientational dependency of the bias even within a single WM fiber bundle, the magnitude of the bias in orientation (θ) and MD ($|\varepsilon_{MD}|$) is visualized for the genu of the corpus callosum, right corticospinal tracts, left cingulum bundle, and left arcuate fasciculus.

In Fig. 6b, the effect of the FA and MD on the bias in the diffusion measures is presented. The two-dimensional frequency plot with respect to FA and MD is also shown

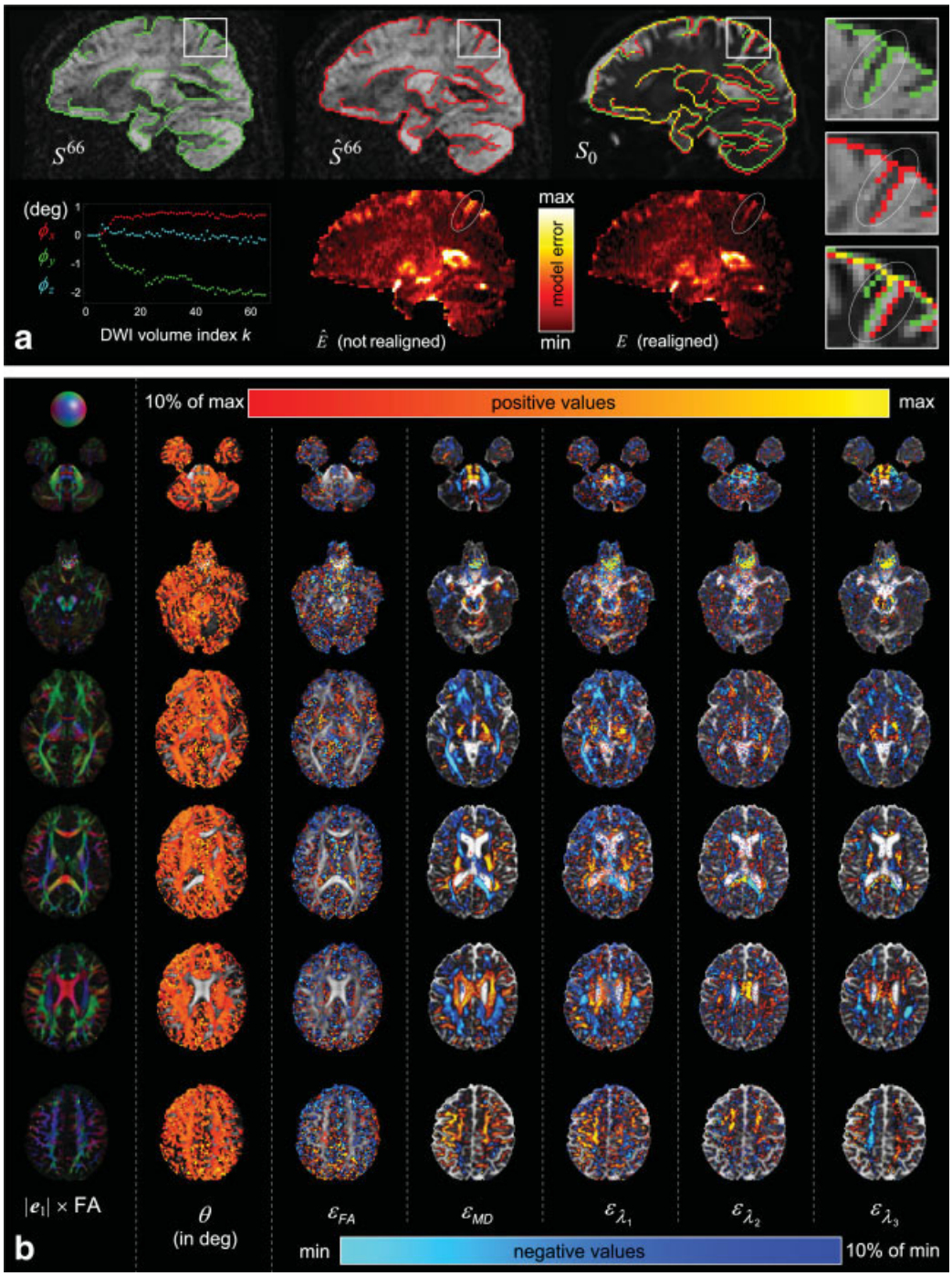

FIG. 5. (**a**) Qualitative (top row and right column) and quantitative (left and middle of bottom row) results from the motion correction procedure. As shown by the encircled region in the enlarged images, overlaying the edges from S^{66} (not realigned) and from $\hat{S}^{66}$ (realigned) to the non-DW image S_0 allows for a clear visual assessment of the realignment quality. This observation is confirmed by a decreased residual model-fit error ($E < \hat{E}$). (**b**) The effect of not reorienting the ***B***-matrix during motion correction on the estimated diffusion measures for a measured DTI data set of a healthy subject. The positive and negative bias are overlayed on the corresponding diffusion map and rendered transparent for values smaller than 10% of their maximum and negative values, respectively. Note that the color maps, which indicate the amount of bias, were scaled differently for each diffusion measure. [Color figure can be viewed in the online issue, which is available at www.interscience.wiley.com.]

(bottom figure) to indicate the region, in which the bias has been estimated robustly (a higher frequency results in a more robust estimation). The bias in all the scalar measures is clearly dependent on the FA and/or the MD.

Error Propagation in Tractography

In Fig. 7a, tracking results in the cingulum are shown with (in red) and without (in yellow) reorienting the

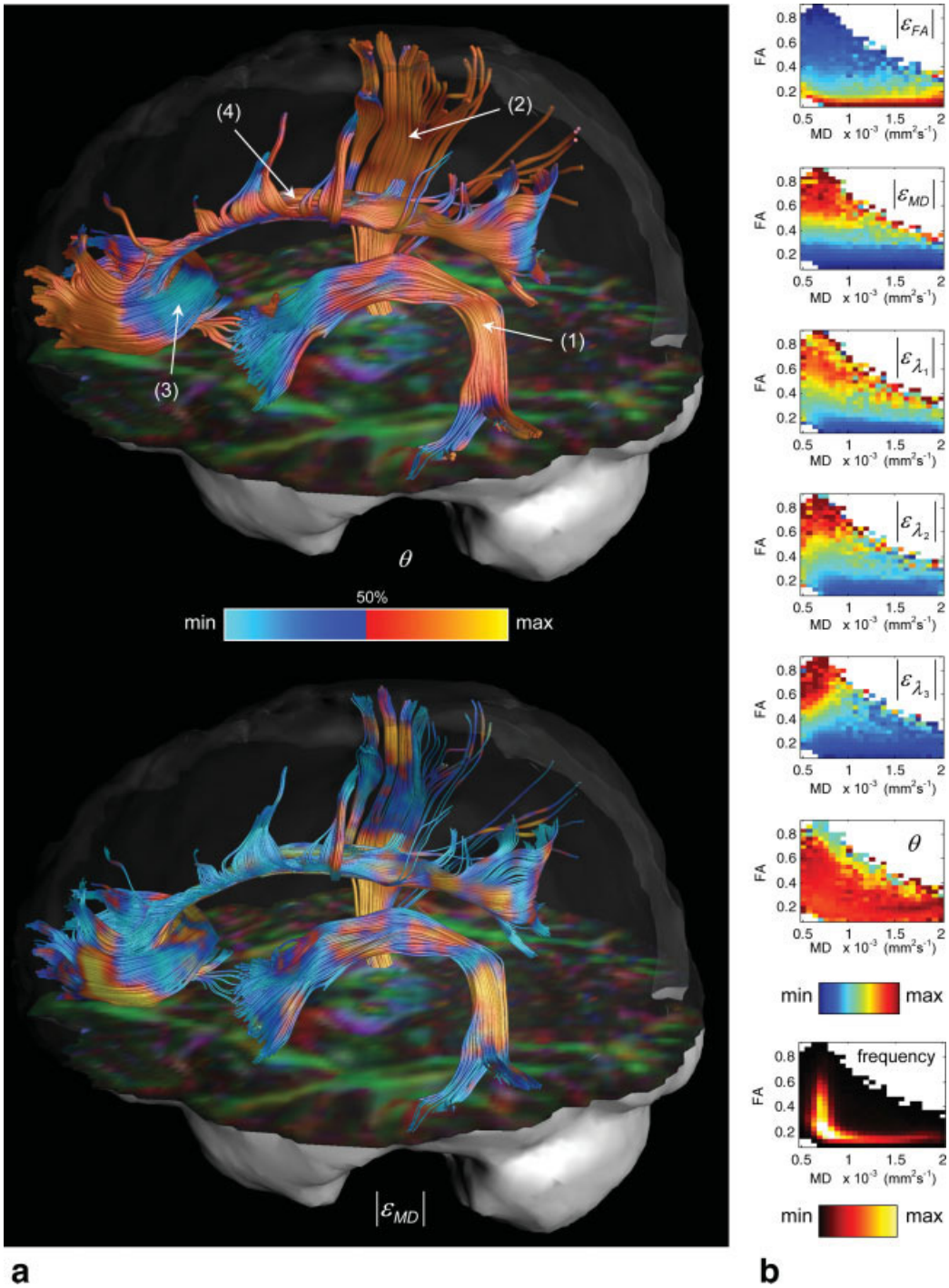

FIG. 6. In (**a**), the bias in orientation of FE (i.e., θ) and the magnitude of the bias in MD (i.e., $|\varepsilon_{MD}|$) are visualized on several WM fiber bundles: the arcuate fasciculus (1), corticospinal tracts (2), genu of the corpus callosum (3), and cingulum (4). In (**b**), the bias in the diffusion measures is shown as a function of the MD and FA. Also, the corresponding frequency plot with respect to FA and MD is shown (bottom figure). Note that the color maps, which indicate the amount of bias, were scaled differently for each diffusion measure.

B-matrix for the deterministic tractography approach. The difference in pathways is clearly visible, especially in the subrostral segment of the cingulum. Similarly, using a probabilistic approach, the spatial distribution of fiber pathways is also affected by omitting the ***B***-matrix rotation as shown in Fig. 7b.

DISCUSSION

Although it has been shown previously that correcting for subject motion and geometrical distortions significantly improves data quality, the majority of researchers still omits the important processing step of reorienting the ***B***-matrix

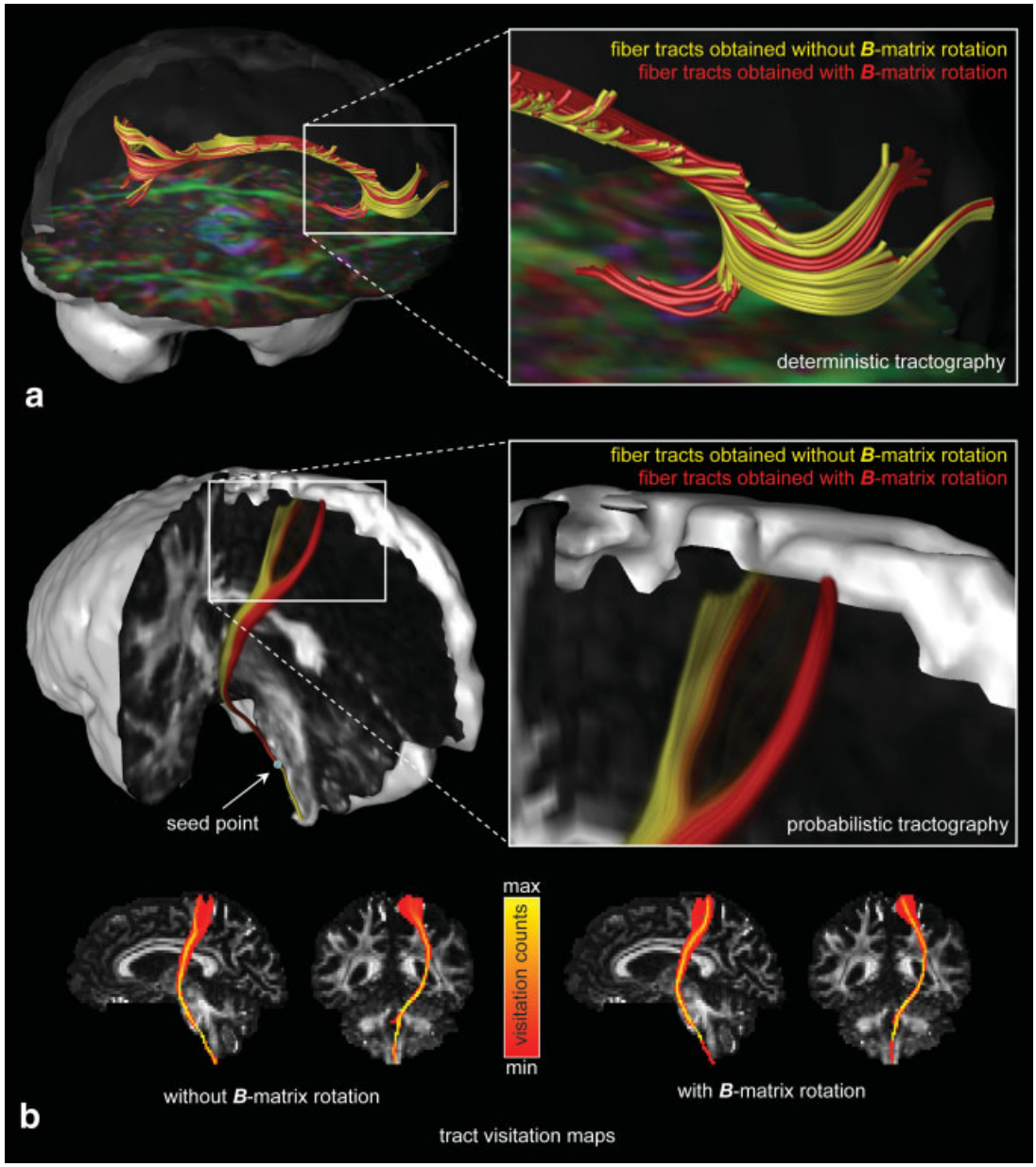

FIG. 7. The effect of neglecting to reorient the ***B***-matrix on the reconstructed fiber tract pathways using a deterministic (**a**) and a probabilistic (**b**) tractography method. [Color figure can be viewed in the online issue, which is available at www.interscience.wiley.com.]

prior to estimating the diffusion tensor. On the basis of literature review of 75 papers published in 2008, in only 33 papers, the application of distortion correction (15 papers), subject motion correction (4 papers), or both (14 papers) was mentioned[1]. In only four papers, rotating the ***B***-matrix was explicitly described (33,35–37).

It is important to note that the approach to correct motion and distortion described in this work is only valid for single-shot data. For multi-shot data, i.e., when parts of *k*-space of a diffusion-weighted image are acquired at different instances with a chance for different diffusion encoding following rotation correction, a more complex tensor estimation needs to be applied (38). In addition, in case of very nonlinear gradients, i.e., head inserts or head only scanners, or when different subjects are placed in different areas of the gradient field (i.e., for group comparisons), translational effects can also cause errors (39).

From correcting subject motion in human brain data, our results show that typical motion patterns resemble a slow drift in head orientation (see Fig. 2a) rather than a random and independent change in head orientation along one or more diffusion gradient directions. This aspect is extremely important as shown by our simulations in Fig. 4b, in which

[1]The literature review was performed using *PubMed* (http://www.ncbi.nlm.nih.gov/pubmed/) with the search terms "diffusion tensor imaging", from which only the relevant papers with in vivo human brain data were selected.

clearly different results are obtained for both types of subject motion: when simulating the head motion as a *random subject motion* with a fixed angle across sampling schemes, a higher bias is obtained when using fewer diffusion gradient directions (34). On the other hand, when modeling subject motion as a random walk in head orientation (i.e., the *subject motion drift*), the opposite situation is observed from our analysis, i.e., a higher number of diffusion gradients results in a larger bias when not rotating the ***B***-matrix. A straightforward explanation for this difference in results is that the random subject motion simulation assumes there is an identical amount of head motion for diffusion sampling schemes that have a different number of gradient directions as opposed to a fixed amount of motion drift per unit time. In doing so, the amount of subject motion is overestimated for sampling schemes with fewer gradient directions, and hence the corresponding bias is overestimated.

Although the *subject motion drift* model describes the experimental measurements more realistically than the *random subject motion* model, further refinements could be incorporated to improve the accuracy of the model, such as twitches, i.e., large head rotations between intervals without (or negligible) subject motion, or settling-in effects due to muscle relaxations. In this context, taking into account population-specific motion patterns (diseased subjects, children, etc. versus healthy volunteers) could even further improve the model reliability.

In our Monte Carlo simulations, no noise was incorporated to disambiguate its effect on the diffusion tensor estimation from the bias due to omitting the ***B***-matrix rotation while correcting for subject motion. Although one could argue that data noise introduces a much higher bias than the bias resulting from not adjusting the ***B***-matrix, our analyses from actual (noisy) human brain data clearly show the significant adverse effect, even for probabilistic tractography, which is driven by the noise distribution itself (Figs. 5b, 6, and 7).

We have demonstrated that neglecting to rotate the ***B***-matrix introduces a bias in the estimated diffusion measures that depends on (1) the amount of motion (Figs. 1 and 2b); (2) the main orientation of subject motion (Figs. 3a,b, 5b, and 6a); (3) the properties of the underlying microstructure as determined by the FE, FA, and MD of the diffusion tensor (Figs. 3c, 4a, and 6b); and (4) the number of gradient directions (Fig. 4b).

It could be argued that the average error in the *scalar* DTI indices (eigenvalues and thus FA, MD, etc.)—induced by not rotating the ***B***-matrix—can be considered relatively small for the example presented in this work. Note, however, that the subject in question was a healthy volunteer familiar with MRI (not knowing this study was about investigation subject motion) who in general moves less than diseased subjects or children. Hence, our results can be considered as highly conservative. The significance of this bias with respect to quantitative studies depends on several interrelated factors:

- The SNR of the acquired data: with a higher SNR, the relative contribution of the variance of the estimated diffusion scalars—induced by not rotating the ***B***-matrix—to the true variance of the underlying signal will become larger, potentially increasing the rate of false negative findings.
- The research question: intra-subject (e.g., laterality) and longitudinal measurements are more sensitive to these errors than group studies, because the induced variance from not rotating the ***B***-matrix might be swamped by the natural variance across multiple subjects. Equivalently, for baseline experiments (important for comparing diseased and healthy subjects), the accuracy might be more important than the precision of the estimated diffusion measures.
- The underlying tissue structural organization and orientation: from both simulations and real measurements, it is clear that the bias depends on the FA, MD, and fiber orientation—and generally, in a nontrivial manner. Consequently, some structures will be affected more adversely.
- The actual motion pattern: simulations and experimental results demonstrate that the amount of bias in a particular structure of interest also depends on the actual direction of head rotation (e.g., pitch versus yaw). This effect of this issue becomes even more important when comparing a group of healthy and diseased subjects, taking into account that patients might move their heads more and differently than healthy subjects.

In general, with higher motion angles, when not rotating the ***B***-matrix, the effect on the scalar DTI indices is generally worse, although nonmonotonous and nonlinear.

In addition to the errors in *scalar* DTI measures, there exists an error in the *directional* diffusion information, i.e., the first eigenvector (and, less importantly here, in the other eigenvectors). Although these errors seem small ($\theta \sim 0.1 - 1$ deg) and therefore perhaps deemed insignificant, our tractography results clearly show the deviation in the reconstructed fiber tract pathways when the ***B***-matrix rotation is not taken into account. Especially the probabilistic tracking result, in which the actual (real) noise distribution is incorporated, is convincing evidence that significantly erroneous tract pathways are reconstructed due to the cumulative propagation of the induced first eigenvector bias (Fig. 7). In this context, it is also important to note that for a large (>20) number of diffusion directions, a drift in head motion is far worse than the occasional (random) head motion (which can be identified as an outlier via robust tensor estimation procedures).

From the 10 subjects studied in this work, it was observed that the pitch tends to be the dominant head rotation for a subject motion drift (bottom Fig. 2a). As a result, WM in commissural pathways—which run predominantly along the left-right axis—is less likely to be affected by this confound. Conversely, WM in the association and projection fibres (which mainly run in the anterior–posterior and superior–inferior directions, respectively) are more susceptible to errors in estimation of the tensor if the ***B***-matrix reorientation is neglected (Fig. 3a). Therefore, our initial data suggests that in both qualitative and quantitative studies, such as voxel-based analysis, false positive, and false negative inferences are more likely to occur in association

and projection fiber pathways if the ***B***-matrix reorientation step is neglected.

CONCLUSIONS

Our results demonstrate that when correcting DW motion artifacts, reorientation of the ***B***-matrix should not be neglected. Failing to perform this simple step introduces a significant bias in diffusion measures and fiber orientation estimates. It is clear that these errors are not uniform: they depend on the relative orientation of the underlying fiber pathways with respect to the main axis of subject rotation and their intrinsic diffusion properties. As a result, not rotating the ***B***-matrix can have potentially disastrous consequences for quantitative DTI and tractography studies where accurate tract reconstructions are necessary (e.g., in surgical planning). It is important to note that the data in this study were collected from highly motivated individuals who understood the need to remain still during data acquisition. In real world (clinical) scenarios, where subjects may be more prone to move during the scan (e.g., due to pathology), the importance of reorienting the ***B***-matrix during motion correction to avoid bias, is even more paramount.

ACKNOWLEDGMENTS

The authors thank Dr. John Evans for the in-depth discussions during this study. In addition, they also thank the referees for reviewing our manuscript with great care. We believe that their constructive comments and suggestions improved the quality of the manuscript significantly.

APPENDIX A

The affine transformation $\boldsymbol{A}$ (for simplicity, the index k is omitted) is defined here as a 4×4 matrix:

$$\boldsymbol{A} = \boldsymbol{T} \cdot \boldsymbol{R} \cdot \boldsymbol{G} \cdot \boldsymbol{S}, \qquad [A1]$$

with the translation matrix $\boldsymbol{T}$ representing the translation parameters t_x, t_y, and t_z along the x, y, and z axis, respectively:

$$\boldsymbol{T} = \begin{bmatrix} 1 & 0 & 0 & t_x \\ 0 & 1 & 0 & t_y \\ 0 & 0 & 1 & t_z \\ 0 & 0 & 0 & 1 \end{bmatrix}, \qquad [A2]$$

the rotation matrix $\boldsymbol{R} = \boldsymbol{R}_x \cdot \boldsymbol{R}_y \cdot \boldsymbol{R}_z$ defined by the rotation angles ϕ_x, ϕ_y, and ϕ_z:

$$\boldsymbol{R}_x = \begin{bmatrix} 1 & 0 & 0 & 0 \\ 0 & \cos(\phi_x) & \sin(\phi_x) & 0 \\ 0 & -\sin(\phi_x) & \cos(\phi_x) & 0 \\ 0 & 0 & 0 & 1 \end{bmatrix}$$

$$\boldsymbol{R}_y = \begin{bmatrix} \cos(\phi_y) & 0 & -\sin(\phi_y) & 0 \\ 0 & 1 & 0 & 0 \\ \sin(\phi_y) & 0 & \cos(\phi_y) & 0 \\ 0 & 0 & 0 & 1 \end{bmatrix}$$

$$\boldsymbol{R}_z = \begin{bmatrix} \cos(\phi_z) & \sin(\phi_z) & 0 & 0 \\ -\sin(\phi_z) & \cos(\phi_z) & 0 & 0 \\ 0 & 0 & 1 & 0 \\ 0 & 0 & 0 & 1 \end{bmatrix}, \qquad [A3]$$

the skew (shear) matrix $\boldsymbol{G}$ described by the parameters g_x, g_y, and g_z:

$$\boldsymbol{G} = \begin{bmatrix} 1 & g_x g_z & g_x & 0 \\ g_y & 1 & 0 & 0 \\ 0 & g_z & 1 & 0 \\ 0 & 0 & 0 & 1 \end{bmatrix}, \qquad [A4]$$

and the scale matrix $\boldsymbol{S}$, which is defined by the scale parameters s_x, s_y, and s_z:

$$\boldsymbol{S} = \begin{bmatrix} s_x & 0 & 0 & 0 \\ 0 & s_y & 0 & 0 \\ 0 & 0 & s_z & 0 \\ 0 & 0 & 0 & 1 \end{bmatrix}. \qquad [A5]$$

APPENDIX B

Two types of subject motion were simulated: (1) *random subject motion* and (2) *subject motion drift*.

1. In Fig. A1a, an example of *random subject motion* was simulated by rotating each diffusion gradient $\hat{\boldsymbol{g}}_k$ with a fixed angle δ of 10° along a random rotation axis, as described in Ref. 34. Note that the orientation of subject motion is independent for each of the resulting diffusion gradients $\boldsymbol{g}_k$.
2. A slow but systematic drift in head orientation, here referred to as *subject motion drift*, was simulated as a random walk along a predefined rotation axis $\boldsymbol{a}$ with a corresponding drift angle along this axis, denoted as $\delta_{\boldsymbol{a}}$. This subject motion drift is computed as follows: given a diffusion sampling scheme of K directions, each diffusion gradient $\hat{\boldsymbol{g}}_k$ is rotated around $\boldsymbol{a}$ by an angle γ_k, which is defined as $\gamma_k = \gamma_{k-1} + \chi$, where χ is randomly sampled from a Gaussian distribution with zero mean and standard deviation $\delta_{\boldsymbol{a}}/\sqrt{K}$ (with $\gamma_0 = 0°$) (40). Figure A1b shows an example of such a simulated subject motion drift around a random axis $\boldsymbol{a} = [1\,1\,0]$ with $K = 10$ and $\delta_{\boldsymbol{a}} = 10°$. In Fig. A1c, the corresponding rotation angles ϕ_x, ϕ_y, and ϕ_z are shown for both examples of subject motion.

The condensed notations δ_{ϕ_x}, δ_{ϕ_y}, and δ_{ϕ_z} will be used when $\boldsymbol{a}$ represents the x-, y-, and z-axis, respectively. On the basis of our experimental findings, the amount of the rotational drifts δ_{ϕ_x}, δ_{ϕ_y}, and δ_{ϕ_z} for a DTI experiment of 60 slices with a 60 directions scheme (with 6 non-DW images), lasting approximately 25 min, typically lies in the range of $[0° \rightarrow 3°]$ and therefore formed the range of angles used in our simulations. The following sections describe the effect of different conditions on the estimation of the diffusion measures when the ***B***-matrix is not rotated when correcting for subject motion.

Effect of Varying Degree of Subject Motion

To illustrate the effect of neglecting to reorient the ***B***-matrix on the estimation of diffusion measures for a single tensor, gradient direction $\hat{\boldsymbol{g}}_1$ from a sampling scheme of 60 isotropically distributed directions was rotated around the z-axis for different rotation angles $\phi_z = [0° \rightarrow 180°]$. Note that this

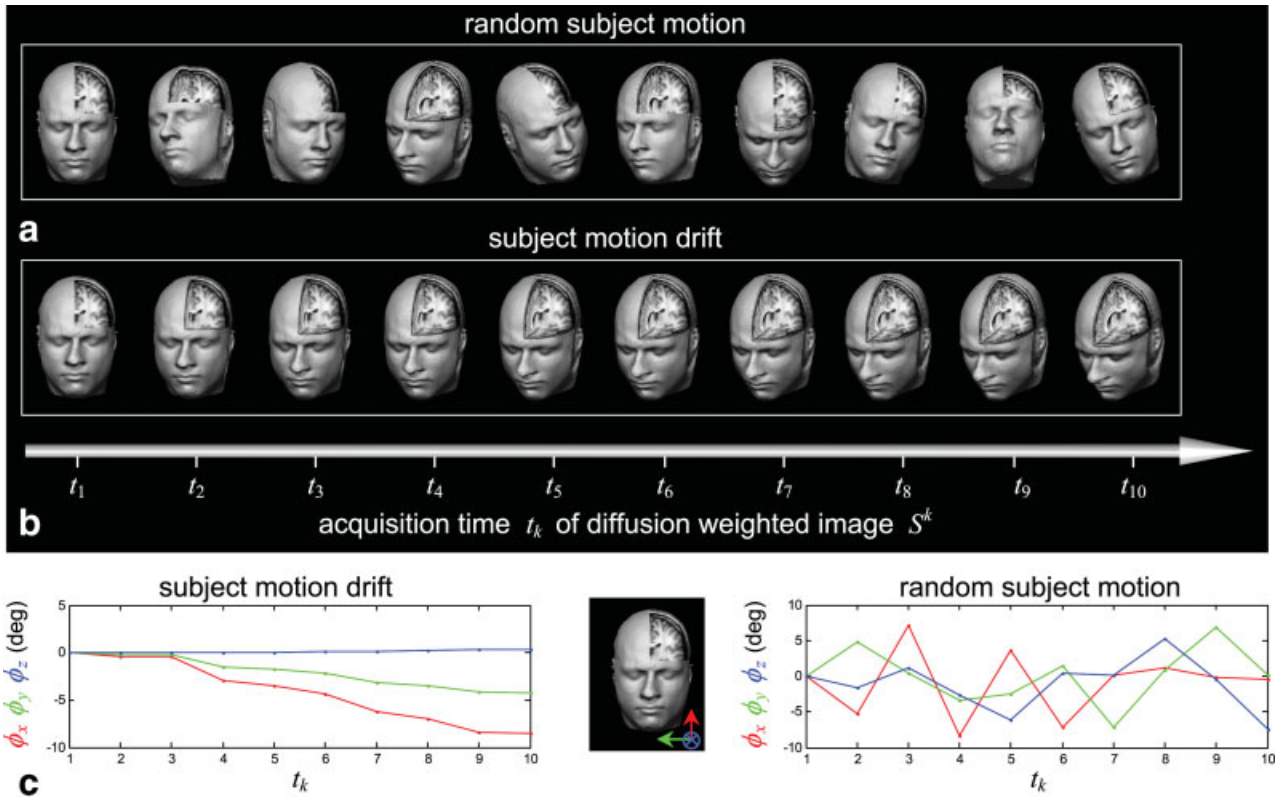

FIG. A1. Two types of head motion are simulated for a diffusion gradient sampling scheme of 10 directions: a *random subject motion*, i.e., a change in head orientation with random rotation axis for each acquisition time t_k, but with a fixed rotation angle (see Ref. 34) (**a**) and arguably a more realistic *subject motion drift*, i.e., a slow and systematic drift in head orientation with a fixed rotation axis for each t_k, but with a rotation angle defined by the random walk procedure. For both examples, the rotation angles are shown in (**c**). [Color figure can be viewed in the online issue, which is available at www.interscience.wiley.com.]

setting reflects a head motion[2] for DW image S^1, but not for the other DW images S^k (with $k = 2, \ldots, 60$). The following parameters were chosen as an illustration: FA = 0.7, MD = 7×10^{-4} mm^2/s, $\boldsymbol{e}_1 = [1\,1\,1]/\sqrt{3}$, and $b = 1200$ s/mm^2. This procedure was also performed for an entire axial slice from a measured data set (with $\phi_z = [1^\circ \rightarrow 3^\circ]$ in steps of 0.25°, and the same b-value, $\hat{\boldsymbol{g}}_1$, and gradient sampling scheme as above).

In addition to the single gradient perturbation, the physically more plausible motion trajectory, i.e., a gradual *subject motion drift*, was simulated. The effect of such a drift along the x-, y-, and z-axis on the corresponding rotation angles ϕ_x, ϕ_y, and ϕ_z is shown by simulating 10 motion trajectories for the 60 directions gradient sampling scheme (and 6 non-DW images) with $\delta_{\phi_\alpha} = 1^\circ$ ($\alpha = x, y, z$).

To demonstrate the effect on the accuracy and precision of the estimated diffusion properties for a single tensor, $N = 1000$ motion drifts are generated with $\delta_{\phi_z} = [0^\circ \rightarrow 3^\circ]$, FA = 0.7, MD = 7×10^{-4} mm^2/s, $\boldsymbol{e}_1 = [1\,1\,1]/\sqrt{3}$, and $b = 1200$ s/mm^2.

Effect of Rotation Axis of Subject Motion

The rotation component of subject motion can be described by rotations in the coronal ($\phi_x \rightarrow$ roll), sagittal ($\phi_y \rightarrow$ pitch), and axial ($\phi_z \rightarrow$ yaw) plane. The effect of rotation axis on diffusion measures is investigated by simulating the predominant subject motion as a roll ($\delta_{\phi_x} = \delta$ and $\delta_{\phi_y} = \delta_{\phi_z} = 0.1^\circ$), pitch ($\delta_{\phi_y} = \delta$ and $\delta_{\phi_x} = \delta_{\phi_z} = \delta$), and yaw ($\delta_{\phi_z} = \delta$ and $\delta_{\phi_x} = \delta_{\phi_y} = 0.1^\circ$) in an entire axial slice with $b = 1200$ s/mm^2, 60 gradient directions, and $\delta = 1^\circ$. This simulation is also performed for a single diffusion tensor with $b = 1200$ s/mm^2, 60 gradient directions, FA = 0.7, MD = 7×10^{-4} mm^2/s, $\boldsymbol{e}_1 = [1\,0.5\,0]/\sqrt{1.25}$, $\delta = [0^\circ \rightarrow 3^\circ]$, and $N = 1000$.

A more general configuration of motion rotation axes $\{\boldsymbol{a}\}$ is simulated by generating a large uniform set of points $\{\boldsymbol{v}\}$ on the unit sphere. Using the same predefined drift pattern $\delta_{\boldsymbol{a}} = 1^\circ$ for each of these axes $\{\boldsymbol{a}\}$, the bias in the FE (i.e., θ) is calculated for $\boldsymbol{e}_1 = [1\,0\,0]$ and $\boldsymbol{e}_1 = [1\,1\,1]/\sqrt{3}$. In addition, for two identical drift patterns $\delta = 1^\circ$ with different rotation axes, i.e., $\boldsymbol{a} = [1\,0\,0]$ and $\boldsymbol{a} = [1\,1\,1]/\sqrt{3}$, the bias θ is computed for a configuration of multiple FE directions that is defined by the same set of points $\{\boldsymbol{v}\}$. Other parameters are as follows: $b = 1200$ s/mm^2, 60 gradient directions, FA = 0.7, MD = 7×10^{-4} mm^2/s.

Effect of Varying Anisotropy and Mean Diffusivity Values

Diffusion tensors with varying magnitude of FA (i.e., $[0.1 \rightarrow 0.9]$) and MD (i.e., $[0.5 \rightarrow 2.5] \times 10^{-3}$ mm^2/s) were generated ($N = 1000$) to simulate the effect of their shape on the accuracy of the estimated diffusion measures when

[2]Although the range of ϕ_z is unrealistic, it is intended to show the nonmonotonic behavior of the bias with increased head motion.

omitting the $\boldsymbol{B}$-matrix reorientation. The following parameters were chosen: $b = 1200$ s/mm^2, 60 gradient directions, $\delta_{\phi_y} = 1°$. A random orientation of $\boldsymbol{e}_1$ was generated for each run.

Diffusion Gradient Sampling Schemes

The effect of the bias on four different gradient sampling schemes (6, 15, 30, and 60 directions) was investigated for (1) the *subject motion drift* and (2) the *random subject motion*.

1. When modeled as a drift, it is obvious that the amount of subject motion—which is constant per unit time—increases for a higher number of gradient directions. Therefore, it is important to note that the amount of drift defined for the 6, 15, and 30 gradient schemes, is computed as if it was predefined for the scheme of 60 gradient directions. Only then, an objective comparison between gradient sampling schemes with fewer directions can be made, effectively taking the duration of the acquisition into account as a normalization for the actual amount of subject motion. The following parameters were used: a drift $\delta = [0° \rightarrow 3°]$ with random orientation of both the drift rotation axis $\boldsymbol{a}$ and $\boldsymbol{e}_1$ for each run, $b = 1200$ s/mm^2, FA = 0.7, MD = 7×10^{-4} mm^2/s, and $N = 1000$.
2. The random subject motion was simulated by rotating each of the original gradient directions for each sampling scheme with a fixed angle $\delta = [0° \rightarrow 3°]$, but with the direction of these rotations being random and independent of each other (34). Other parameters were identical as in (1).

REFERENCES

1. Skare S, Li T, Nordell B, Ingvar M. Noise considerations in the determination of diffusion tensor anisotropy. Magn Reson Imaging 2000;18:659–669.
2. Anderson AW. Theoretical analysis of the effects of noise on diffusion tensor imaging. Magn Reson Med 2001;46:1174–1188.
3. Basser PJ, Pajevic S. A normal distribution for tensor-valued random variables: applications to diffusion tensor MRI. IEEE Trans Med Imag 2003;22:785–794.
4. Pajevic S, Basser PJ. Parametric and non-parametric statistical analysis of DT-MRI data. J Magn Reson 2003;161:1–14.
5. Jones DK, Basser PJ. Squashing peanuts and smashing pumpkins: How noise distorts diffusion-weighted MR data. Magn Reson Med 2004;52:979–993.
6. Rohde GK, Barnett AS, Basser PJ, Marenco S, Pierpaoli C. Comprehensive approach for correction of motion and distortion in diffusion-weighted MRI. Magn Reson Med 2004;51:103–114.
7. Kim DJ, Park HJ, Kang KW, Shin YW, Kim JJ, Moon WJ, Chung EC, Kim IY, Kwon JS, Kim SI. How does distortion correction correlate with anisotropic indices? A diffusion tensor imaging study. Magn Reson Imaging 2006;24:1369–1376.
8. Alexander AL, Tsuruda JS, Parker DL. Elimination of eddy current artifacts in diffusion-weighted echo-planar images: the use of bipolar gradients. Magn Reson Med 1997;38:1016–1021.
9. Papadakis NG, Martin KM, Pickard JD, Hall LD, Carpenter TA, Huang CL. Gradient pre-emphasis calibration in diffusion weighted echo-planar imaging. Magn Reson Med 2000;44:616–624.
10. Mangin JF, Poupon C, Clark CA, Le Bihan D, Bloch I. Distortion correction and robust tensor estimation for MR diffusion imaging. Med Image Anal 2002;6:191–198.
11. Nielsen JF, Ghugre NR, Panigrahy A. Affine and polynomial mutual information coregistration for artifact elimination in diffusion tensor imaging of newborns. Magn Reson Imaging 2004;22:1319–1323.
12. Jezzard P, Barnett AS, Pierpaoli C. Characterization of and correction for eddy current artifacts in echo planar diffusion imaging. Magn Reson Med 1998;39:801–812.
13. Bastin ME, Armitage PA. On the use of water phantom images to calibrate and correct eddy current induced artefacts in MR diffusion tensor imaging. Magn Reson Imaging 2000;18:681–687.
14. Andersson JLR, Skare S. A model-based method for retrospective correction of geometric distortions in diffusion-weighted EPI. NeuroImage 2002;16:177–199.
15. Ardekani S, Sinha U. Geometric distortion correction of high-resolution 3 T diffusion tensor brain images. Magn Reson Med 2005;54:1163–1171.
16. Farrell JA, Landman BA, Jones CK, A SS, Prince JL, van Zijl PC, Mori S. Effects of signal-to-noise ratio on the accuracy and reproducibility of diffusion tensor imaging-derived fractional anisotropy, mean diffusivity, and principal eigenvector measurements at 1.5 T. J Magn Reson Imaging 2007;26:756–767.
17. Landman BA, Farrell JA, Jones CK, Smith SA, Prince JL, Mori S. Effects of diffusion weighting schemes on the reproducibility of dti-derived fractional anisotropy, mean diffusivity, and principal eigenvector measurements at 1.5 T. NeuroImage 2007;36:1123–1138.
18. Jansen JF, Kooi ME, Kessels AG, Nicolay K, Backes WH. Reproducibility of quantitative cerebral T2 relaxometry, diffusion tensor imaging, and 1H magnetic resonance spectroscopy at 3.0 tesla. Invest Rediol 2007;42:327–337.
19. Jones DK, Horsfield MA, Simmons A. Optimal strategies for measuring diffusion in anisotropic systems by magnetic resonance imaging. Magn Reson Med 1999;42:515–525.
20. Papadakis NG, Xing D, Huang CLH, Hall LD, Carpenter TA. A comparative study of acquisition schemes for diffusion tensor imaging using MRI. J Magn Reson 1999;137:67–82.
21. Skare S, Hedehus M, Moseley ME, Li TQ. Condition number as a measure of noise performance of diffusion tensor data acquisition schemes with MRI. J Magn Reson 2000;147:340–352.
22. Jones DK. The effect of gradient sampling schemes on measures derived from diffusion tensor MRI: A Monte Carlo study. Magn Reson Med 2004;51:4607–4621.
23. Papadakis NG, Murrills CD, Hall LD, Huang CLH, Carpenter TA. Minimal gradient encoding for robust estimation of diffusion anisotropy. Magn Reson Imaging 2000;18:671–679.
24. Batchelor PG, Atkinson D, Hill DL, Calamante F, Connelly A. Anisotropic noise propagation in diffusion tensor MRI sampling schemes. Magn Reson Med 2003;49:1143–1151.
25. Dubois J, Poupon C, Lethimonnier F, Le Bihan D. Optimized diffusion gradient orientation schemes for corrupted clinical DTI data sets. MAGMA 2006;19:134–143.
26. Cook PA, Symms M, Boulby PA, Alexander DC. Optimal acquisition orders of diffusion-weighted MRI measurements. J Magn Reson Imaging 2007;25:1051–1058.
27. Clark CA, Barrick TR, Murphy MM, Bell BA. White matter fiber tracking in patients with space-occupying lesions of the brain: A new technique for neurosurgical planning? NeuroImage 2003;20:1601–1608.
28. Kinoshita M, Yamada K, Hashimoto N, Kato A, Izumoto S, Baba T, Maruno M, Nishimura T, Yoshimine T. Fiber-tracking does not accurately estimate size of fiber bundle in pathological condition: Initial neurosurgical experience using neuronavigation and subcortical white matter stimulation. NeuroImage 2005;25:424–429.
29. Yu CS, Li KC, Xuan Y, Ji XM, Qin W. Diffusion tensor tractography in patients with cerebral tumors: A helpful technique for neurosurgical planning and postoperative assessment. Eur J Radiol 2005;56:197–204.
30. Marquardt D. An algorithm for least-squares estimation of nonlinear parameters. Siam J Appl Math 1963;11:431–441.
31. Maes F, Collignon A, Vandermeulen D, Marchal G, Suetens P. Multimodality image registration by maximization of mutual information. IEEE Trans Med Imag 1997;16:187–198.
32. Basser PJ, Pajevic S, Pierpaoli C, Duda J, Aldroubi A. In vivo fiber tractography using DT-MRI data. Magn Reson Med 2000;44:625–632.
33. Jones DK. Tractography gone wild: Probabilistic fibre tracking using the wild bootstrap with diffusion tensor MRI. IEEE Trans Med Imag 2008;27:1268–1274.
34. Maniega SM, Bastin ME, Armitage PA. Effects of random subject rotation on optimised diffusion gradient sampling schemes in diffusion tensor MRI. Magn Reson Imaging 2008;26:451–460.

35. Pasternak O, Assaf Y, Intrator N, Sochen N. Variational multiple-tensor fitting of fiber-ambiguous diffusion-weighted magnetic resonance imaging voxels. Magn Reson Imaging 2008;26:1133–1144.
36. Klöppel S, Bäumer T, Kroeger J, Koch MA, Büchel C, Münchau A, Siebner HR. The cortical motor threshold reflects microstructural properties of cerebral white matter. NeuroImage 2008;40:1782–1791.
37. Landman BA, Farrell JA, Huang H, Prince JL, Mori S. Diffusion tensor imaging at low SNR: Nonmonotonic behaviors of tensor contrasts. Magn Reson Imaging 2008;26:790–800.
38. Aksoy M, Liu C, Moseley ME, Bammer R. Single-step nonlinear diffusion tensor estimation in the presence of microscopic and macroscopic motion. Magn Reson Med 2008;59:1138–1150.
39. Bammer R, Markl M, Barnett A, Acar B, Alley MT, Pelc NJ, Glover GH, Moseley ME. Analysis and generalized correction of the effect of spatial gradient field distortions in diffusion-weighted imaging. Magn Reson Med 2003;50:560–569.
40. Spitzer F. Principles of random walk, 2nd ed. Berlin; Springer: 1976.